Intense-Laser Solid State Physics: Unraveling the Difference between Semiconductors and Dielectrics

C. R. McDonald,[1,*] G. Vampa,[1] P. B. Corkum,[1,2] and T. Brabec[1]
[1]Department of Physics, University of Ottawa, Ottawa, Ontario K1N 6N5, Canada
[2]National Research Council of Canada, Ottawa, Ontario K1A 0R6, Canada

(Received 16 January 2016; revised manuscript received 22 February 2017; published 24 April 2017)

Experiments on intense laser driven dielectrics have revealed population transfer to the conduction band to be oscillatory in time. This is in stark contrast to ionization in semiconductors and is currently unexplained. Current ionization theories neglect coupling between the valence and conduction band and therewith, the dynamic Stark shift. Our single-particle analysis identifies this as a potential reason for the different ionization behavior. The dynamic Stark shift increases the band gap with increasing laser intensities, thus suppressing ionization to an extent where virtual population oscillations become dominant. The dynamic Stark shift plays a role dominantly in dielectrics which, due to the larger band gap, can be exposed to significantly higher laser intensities.

DOI: 10.1103/PhysRevLett.118.173601

For 50 years, Keldysh theory [1] has been the standard approach for modeling the response of solids to intense under-resonant laser fields. The dominant response revealed by Keldysh theory is optical field ionization—transitions creating electrons (holes) in the conduction (valence) band. Whereas measurements of ionization in semiconductors [2] are consistent with Keldysh theory, recent experiments [3–6] indicate that it needs to be amended for dielectrics; they show mainly an oscillatory population exchange between the valence and conduction band and little ionization.

Progress has been made with generalizations of Keldysh theory, revealing some of its limitations [7–9]. Nevertheless, the physics responsible for the fundamental difference between ionization in semiconductors and in dielectrics remains unresolved. As ionization is the first step in all strong field experiments, this deficiency impedes progress in a wide range of topical areas: (i) material machining [10–13], (ii) petahertz optoelectronics [4,5], and (iii) attosecond condensed matter physics [6,14–20].

Current ionization theories start from the two-band semiconductor Bloch equations [21]. The four most notable approximations used are a semi-infinite band gap [1], the quasicontinuous wave approximation [1,7,9], the frozen valence band approximation [1,7–9], and the neglect of many-body effects [1,7–9]. Recent experiments have shown that the single-particle two-band model gives a satisfactory description of high-harmonic generation in semiconductors [19,20]. Given this fact and the complexity of full many-body theory, it stands to reason to first investigate single-particle approximations.

We examine ionization using the full two-band (2B) model, the frozen valence band (FVB) model, and a generalized Keldysh (GK) model developed here. The GK model relies on the FVB and quasicontinuous wave approximations and permits application of Keldysh theory to arbitrary band gaps. Semiconductors (dielectrics) are represented by a nearest-neighbor model in the limits of a small (wide) band gap and wide (narrow) bandwidth. These two limits reveal dramatically different physics. The model semiconductor agrees with the original Keldysh theory. By contrast, the dielectric shows a wealth of phenomena lying beyond Keldysh theory; their origins are identified by comparing our various models.

We find that ionization can terminate through the closing of all integer photon channels in long pulses, and non-integer photon channels can play a dominant role in short pulses. Our main finding with regard to recent dielectric experiments [3–5] is a potential mechanism explaining their unexpected ionization behavior; the dynamic Stark shift suppresses ionization by widening the band gap with increasing laser intensity. It affects predominantly large band gap materials, which can be exposed to higher intensities. This effect is lost in all FVB models neglecting valence band dynamics. Because of ionization suppression, virtual population oscillations become dominant.

We start from the full 2B equations

$$\partial_t b_v(\mathbf{K},t) = i\Omega(\mathbf{K},t) b_c(\mathbf{K},t) e^{-iS(\mathbf{K},t)}, \tag{1a}$$

$$\partial_t b_c(\mathbf{K},t) = i\Omega^*(\mathbf{K},t) b_v(\mathbf{K},t) e^{iS(\mathbf{K},t)}, \tag{1b}$$

where b_v and b_c are the probability amplitudes of the valence and conduction band [22–24], respectively, and $S(\mathbf{K},t) = \int_{-\infty}^{t} \varepsilon(\mathbf{K}+\mathbf{A}(t'))dt'$, with band gap ε and vector potential $\mathbf{A}(t) = -\hat{z}(F_0/\omega_0) f(t/\tau_0)\sin(\omega_0 t)$; the electric field is $\mathbf{F}(t) = -d\mathbf{A}/dt$. Here, F_0 is the peak field, ω_0 the circular frequency, $T_0 = 2\pi/\omega_0$ the oscillation period, and f the pulse envelope, with τ_0 the FWHM. Further, crystal momentum $\mathbf{k} = \mathbf{K} + \mathbf{A}(t)$ and Brillouin

zone $\overline{\mathrm{BZ}} = \mathrm{BZ} - \mathbf{A}(t)$ have been transformed into a frame moving with $\mathbf{A}(t)$. We denote $\mathbf{k} = (k, \mathbf{k}_\perp)$ and $\mathbf{K} = (K, \mathbf{k}_\perp)$, with $k = K + A(t)$ and $\mathbf{k}_\perp$ crystal momenta parallel and perpendicular to laser polarization, respectively. Finally, $\Omega(\mathbf{K}, t) = \mathbf{d}(\mathbf{K} - \mathbf{A}(t)) \cdot \mathbf{F}(t)$, with $\mathbf{d}$ the dipole between the bands. In what follows, we outline the development of the GK model; see Supplemental Material [24] for more details.

The band gap $\varepsilon(\mathbf{k}) = \overline{E}_g + \varepsilon_\parallel(k)$ is the difference between conduction and valence bands; here, $\overline{E}_g = E_g + \varepsilon_\perp(\mathbf{k})$, with E_g the minimum band gap and $\varepsilon_\perp$ a general band gap orthogonal to the laser polarization. The band gap along laser polarization is given by $\varepsilon_\parallel(k) = \sum_{j=0}^{\infty} \alpha_j \cos(jka)$, where a is the lattice constant; the bandwidth is $\Delta = \max[\varepsilon_\parallel(k)]$.

The exponent in Eqs. (1) consists of sinusoidal and nonsinusoidal contributions, $S = S_s + S_{\mathrm{ns}}$. From the Fourier-Bessel expansion $S_{\mathrm{ns}} = \int_{-\infty}^{t} dt' \varepsilon_{\mathrm{ns}}(t')$, where $\varepsilon_{\mathrm{ns}} = \overline{E}_g + \sum_{j=0}^{\infty} \alpha_j \cos(jKa) J_0(j\beta f(t/\tau_0))$ is the nonsinusoidal part of the laser dressed band gap, with J_0 a Bessel function of the first kind and $\beta = F_0 a/\omega_0$. From Eq. 1(b), we define

$$L(\mathbf{K}, t) = \Omega^*(\mathbf{K}, t) b_v(\mathbf{K}, t) e^{iS_s(\mathbf{K}, t)} \tag{2}$$

and connect with Keldysh theory by splitting $L(\mathbf{K}, t) = \sum_n L_n(\mathbf{K}, t) \exp(-in\sigma t)$ into contributions from finite frequency bands σ, where

$$L_n(\mathbf{K}, t) = \frac{\sigma}{2\pi} \int_{-\infty}^{\infty} dt' L(\mathbf{K}, t') e^{in\sigma t'} \mathrm{sinc}\left(\frac{\sigma}{2\pi}(t - t')\right), \tag{3}$$

and $\mathrm{sinc}(x) = \sin(\pi x)/(\pi x)$. The conduction band population is then

$$n_c(t) = \int_{\overline{\mathrm{BZ}}} d^3K \left| \sum_{n=-\infty}^{\infty} \int_{-\infty}^{t} dt' L_n(\mathbf{K}, t') R_n(\mathbf{K}, t') \right|^2, \tag{4}$$

with $R_n(\mathbf{K}, t) = \exp(iS_{\mathrm{ns}}(\mathbf{K}, t) - in\sigma t)$. The Keldysh-type Eq. (4) is identical to $n_c = \int_{\overline{\mathrm{BZ}}} d^3K |b_c|^2$, obtained from (1). Its main virtue lies in providing a basis for analyzing ionization. GK ionization theory is obtained by applying the following approximations to Eq. (4).

Approximation 1 (FVB) relies on setting $b_V(\mathbf{K}, t) \approx b_V(t = -\infty) = b_0$ in Eq. (2); changes in the valence band are assumed to be negligible [1,25].

Approximation 2 (quasicontinuous wave) applies when the pulse envelope changes a little over one oscillation period so that the envelope $f(t_s/\tau_0)$ in Eq. (3) can be assumed to be constant; here, t_s is a slowly varying time. By considering only the t dependence of the rapidly varying sinusoidal functions and by choosing $\sigma = \omega_0$, the integral in Eq. (3) becomes a Fourier series integral $L_n(\mathbf{K}, t_s) = (\omega_0/2\pi) \int_{-T_0/2}^{T_0/2} dt' L(\mathbf{K}, t_s, t') e^{in\omega_0 t'}$. The remaining time integral $|\int_{-\infty}^{t} dt' R_n(\mathbf{K}, t_s, t')|^2 \to 2\pi t \delta[\varepsilon_{\mathrm{ns}}(\mathbf{K}, t_s) - n\omega_0]$. This gives nonzero results only for resonant n-photon channels satisfying energy conservation

$$\overline{E}_g + \sum_{j=0}^{\infty} \alpha_j \cos(jKa) J_0(j\beta f(t_s/\tau_0)) - n\omega_0 = 0. \tag{5}$$

Condition (5) determines crystal momenta at which the photon energy $n\omega_0$ is equal to the nonsinusoidal part of the laser dressed band gap $\varepsilon_{\mathrm{ns}}$, see Figs. 1(g)–1(j). The ionization dynamics of each channel, such as the different intensity scaling of ionization in the multiphoton and tunneling regimes, is defined by L_n. We solve Eq. (5) for $K = K_n(\beta, \mathbf{k}_\perp, t_s)$. As different n's result in different K_n's, products of L_n and $L_{n'}$ do not overlap in K space and are zero in Eq. (4). Real values of K_n represent ionization; i.e., n_c exhibits net growth after the laser pulse. The other (complex) channels are neglected in Keldysh theory. As energy is not conserved, they contribute to virtual population dynamics and do not yield net growth of n_c after the laser pulse. The number of resonant channels and their dynamic evolution can substantially differ from Keldysh theory [7]; this difference will come from approximation 3 below. In the weak field limit, the number of resonant channels is $n_r = \lfloor \Delta/\omega_0 \rfloor$, and the lowest channel number is $n_1 = \lceil E_g/\omega_0 \rceil$, giving a set of integer number resonant channels $N_r = \{n \in \mathbb{N} | n_1 \le n \le n_1 + n_r - 1\}$. Laser dressing of the band gap can reduce the number of channels. Depending on the argument of J_0, some or all of the K_n may turn complex, rendering these channels closed to ionization [26].

Using the δ function, the integral dK in (4) is evaluated, yielding

$$\frac{dn_c}{dt_s} = 2\pi \int_{\mathrm{BZ}_\perp} d\mathbf{k}_\perp \sum_{n \in N_r} \frac{|L_n(\mathbf{K}_n, t_s)|^2}{|\varepsilon'_{\mathrm{ns}}(\mathbf{K}_n, t_s)|}, \tag{6a}$$

$$L_n(\mathbf{K}_n, t_s) = \frac{\omega_0 b_0}{2\pi} \int_{-\frac{T_0}{2}}^{\frac{T_0}{2}} dt' [\Omega^* e^{iS}](\mathbf{K}_n, t_s, t'), \tag{6b}$$

where $\mathbf{K}_n = (K_n, \mathbf{k}_\perp)$, $\varepsilon'_{\mathrm{ns}} = d\varepsilon_{\mathrm{ns}}/dK$, and $\mathrm{BZ}_\perp$ is the Billouin zone orthogonal to laser polarization. For 1D models, $\mathbf{k}_\perp = 0$, and the integral $d\mathbf{k}_\perp$ vanishes. For general 3D band gaps, the integral $d\mathbf{k}_\perp$ can be approximately evaluated analytically [24].

Approximation 3 applies to the semi-infinite band gap model used by Keldysh. Here, we use a finite band gap, which is essential to understand ionization in dielectrics.

The above models are used to study ionization in a 1D model semiconductor and dielectric with nearest-neighbor band structure, where $\alpha_0 = -\alpha_1 = \Delta/2$ and $\alpha_j = 0$ for $j \ge 2$. We use a narrow (wide) band gap and wide (narrow) bandwidth for semiconductors (dielectrics).

Figures 1(a) and 1(b) show the final conduction band population in the semiconductor versus β, using the 2B

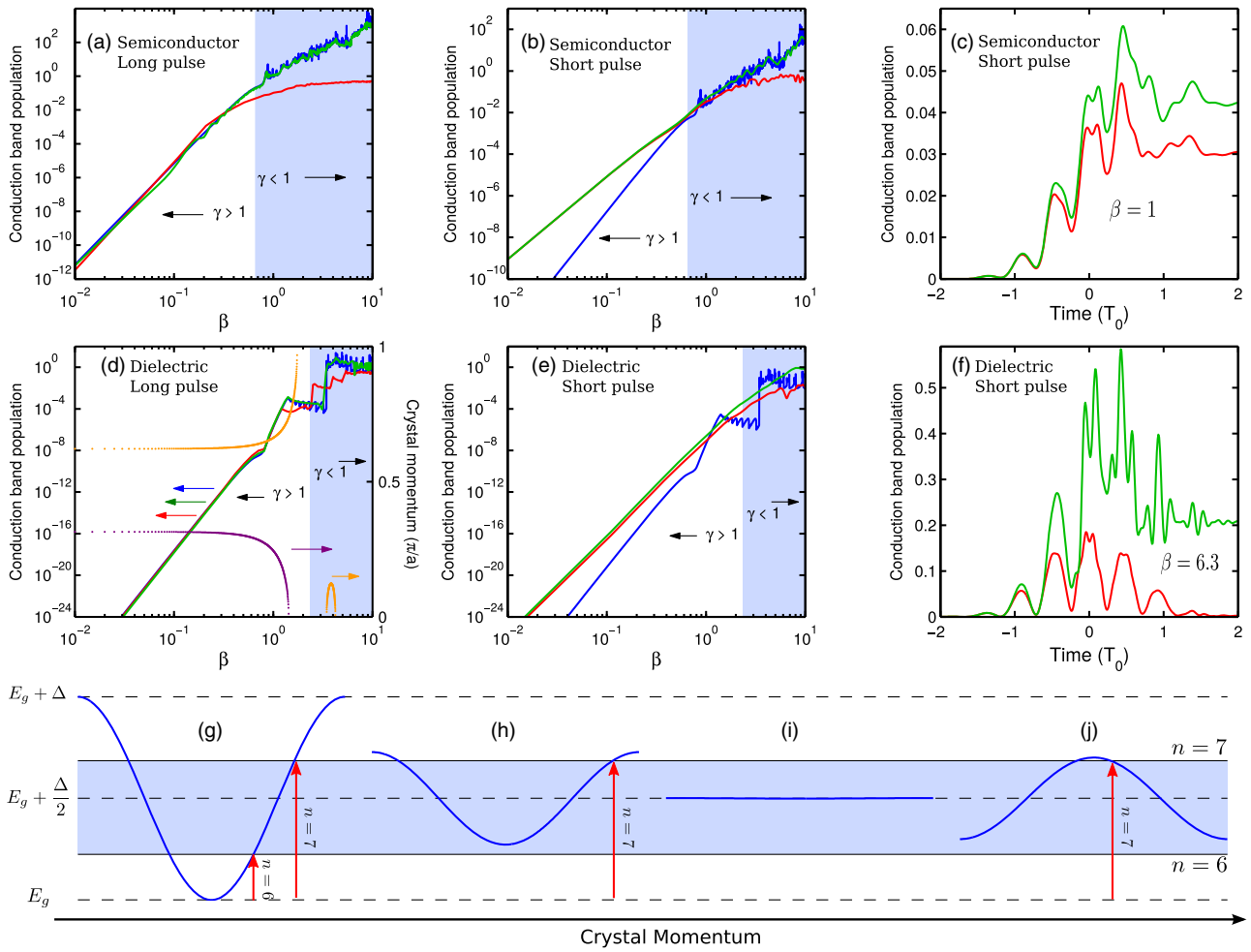

FIG. 1. Top (a)–(c): Ionization in a semiconductor, with $E_g = 0.129$ a.u., $\Delta = 0.6$ a.u., $a = 5.32$ a.u., $d = 3.46$ a.u. for a long (a) and short (b),(c) pulse. Middle (d)–(f): Ionization in a dielectric with $E_g = 0.33$ a.u., $\Delta = 0.13$ a.u., $a = 9.45$ a.u., $d = 5.66$ a.u. for a long (d) and short (e),(f) pulse. (a),(b),(d),(e) Final conduction band population versus $\beta = F_0 a/\omega_0$; the shaded region marks where the Keldysh parameter $\gamma = (\omega_0/F_0 a)\sqrt{2E_g/\Delta} < 1$. (c) Time evolution for the short pulse in (b) at $\beta = 1$. (f) Time evolution for the short pulse in (e) at $\beta = 6.3$. The laser field has $\omega_0 = 0.06$ a.u. and a Gaussian envelope with width $\tau_0 = 100T_0$ for the long pulse (a),(d) and $\tau_0 = 1.7T_0$ for the short pulse (b),(e). The colors in (a)–(f) show the 2B solution (red), the FVB solution (green), and the GK solution (blue). Further, (d) shows the position of K_n for $n = 6$ (purple) and $n = 7$ (orange); the colored arrows indicate the y axis to which the line of corresponding color belongs. Bottom (g)–(j): Illustration of the resonance condition in Eq. (5), where $\varepsilon_{\rm ns}$ (blue lines) is shown for $\beta = 0.0, 1.5, 2.4, 4.2$. The solid lines and arrows show the $n = 6$ and $n = 7$ resonances. The intersection between blue curves and solid lines gives the position of K_n; in the absence of an intersection, the channel is closed.

Eq. (1) (red), FVB Eq. (1b), with $b_v(t) = b_0$ (green), and GK Eq. (6) (blue) for a long (a) and short (b) pulse, respectively. The overall agreement of all three approaches is good. Differences exist at large β, where the valence band is emptied ($n_c \to 1$). Because of the quasicontinuous wave assumption, GK also underestimates short pulse ionization in the multiphoton limit, where the Keldysh parameter is $\gamma \gg 1$, see 1(b). The broad pulse spectrum permits ionization to proceed via all frequency channels within the band, not just at $n\omega_0$. Thus, channels exist that are not accounted for by GK theory. Figure 1(c) shows the subcycle dynamics for $\beta = 1$ in 1(b) for the 2B (red) and FVB (green) solutions. Ionization proceeds stepwise at each half cycle, as expected from conventional ionization theory and in agreement with the experiment [2].

Figures 1(d)–1(f) are the corresponding calculations for the dielectric. We first focus on the GK and FVB results in 1(d) (long pulse), which agree well. The ionization characteristics for the dielectric (d) and semiconductor (a) for larger β are markedly different. This difference is due, in large part, to the difference in material bandwidths. At $\beta = 0$, the semiconductor bandwidth has channels $N_r = \{3, \ldots, 12\}$, whereas, the dielectric has $N_r = \{6, 7\}$. The small number of ionizing channels in the dielectric results in wide ranges of β for which all channels are closed. This is demonstrated by the purple ($n = 6$) and orange ($n = 7$)

lines in Fig. 1(d), which show K_n versus β; ionization terminates when there are no real K_n solutions. The large jump in ionization coincides with the reopening and reclosing of channel $n = 7$ (see orange line). This description is complemented by Figs. 1(g)–1(j), where the resonance condition in Eq. (5) is depicted. Termination of ionization can never happen in Keldysh theory as a result of the semi-infinite band gap model. For the large number of channels available to the semiconductor, complete channel closing is unlikely. The 2B solution also reflects the same physics as the FVB and GK solutions; however, the channel closing characteristics are altered.

The GK approach is inadequate for modeling the short pulse ionization dynamics in a dielectric, see Fig. 1(e). In Fig. 1(e), the FVB and 2B plots show similar behavior, with the 2B result being about two orders of magnitude lower than the FVB result at high fields. However, Fig. 1(f) demonstrates the inadequacy of the FVB solution to model the short pulse ionization dynamics in a dielectric. It depicts the time evolution of n_c for $\beta = 6.3$ in Fig. 1(e), which is close to the highest intensity used in Ref. [3]. The 2B solution shows mostly oscillations with very little final conduction band population in agreement with experiment [3], whereas the FVB solution significantly overstates ionization. The population oscillations arise from the nonresonant (virtual) terms in Eq. (4). In what follows, we will examine (i) how ionization occurs in dielectrics exposed to short pulses and (ii) what suppresses ionization in the 2B model.

Short pulses supply a continuum of frequencies, allowing transitions to occur over the whole Brillouin zone, not only at discrete K_n's. As such, ionization dynamics for $\beta = 1.6$ and 6.3 in Fig. 1(e) are decomposed into frequency bands in Figs. 2(a) and 2(b), respectively. This is done by using Eq. (4), with bands $\sigma = \omega_0/2$ centered at $6\omega_0$ (solid), $6.5\omega_0$ (dashed), and $7\omega_0$ (dotted); cross terms between bands are negligible. When $\beta = 1.6$, the $6\omega_0$ band is the dominant contributor to ionization; however, there is also a significant contribution from the channels around $6.5\omega_0$, which is not included in Keldysh theory. For $\beta = 6.3$, growth of the $6\omega_0$ and $7\omega_0$ bands is impeded by channel closings. The $6.5\omega_0$ channel becomes the dominant pathway for ionization. This results from the frequency at $\omega = E_g + \Delta/2 = 6.6\omega_0$, the only part of $\varepsilon_{\rm ns}$ that never disappears, see Figs. 1(g)–1(j). As this frequency can be reached by the wide pulse spectrum, the $6.5\omega_0$ channel never closes and outgrows the others. The corresponding FVB calculations show similar physics—albeit with higher ionization—and hence, are not shown.

So far, we have discussed the physical processes through which ionization occurs. These processes are the same for the 2B and FVB models; however, from Fig. 1(f), it is apparent that ionization in the 2B model is suppressed by two orders of magnitude relative to the FVB model, whereas, the virtual population oscillations differ by approximately a factor of two. In what follows, we explain this discrepancy. Significant suppression of ionization in the 2B model happens for $n_c \ll 1$ so that depletion can be ruled out as a cause. Coupling between the bands, as occurs in the 2B model, leads to a dynamic Stark shift, increasing their energy difference to $(E_g^2 + \Omega^2)^{1/2}$ [21,27]. A larger band gap results in less ionization. This is verified in Fig. 3, where final n_c is plotted versus Ω_r/E_g. The peak Rabi frequency $\Omega_r = dF_0$ is varied by changing d. The full and dash-dotted lines represent the 2B and FVB solutions. For $\Omega_r/E_g \ll 1$, the two solutions agree, while for $\Omega_r/E_g \sim 1$, 2B ionization is suppressed. The same effect is also responsible for the differences in channel opening and closing and for the smaller jumps in the 2B solution in the long pulse limit in Fig. 1(d). The dynamic Stark shift is less relevant in semiconductors, where the smaller band gap limits exposure to significantly weaker fields.

In conclusion, ionization of dielectrics in near-IR lasers was found to be strongly influenced by channel closing and dynamic Stark effect. These effects depend strongly on pulse shape and parameters, thus opening the potential for coherent control of optical field ionization in dielectrics. How will they change for longer wavelengths?

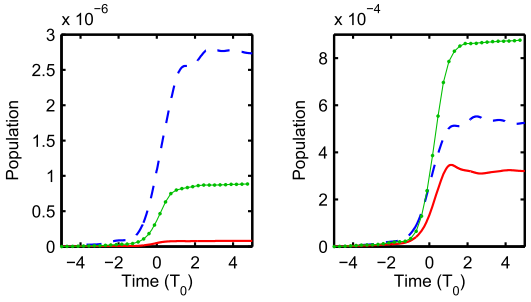

FIG. 2. Short pulse time dynamics in the dielectric for the channels centered around $6\omega_0$ (dashed), $6.5\omega_0$ (dotted), and $7\omega_0$ (solid) for (a) $\beta = 1.6$ and (b) $\beta = 6.3$; for all other parameters, see Fig. 1(e).

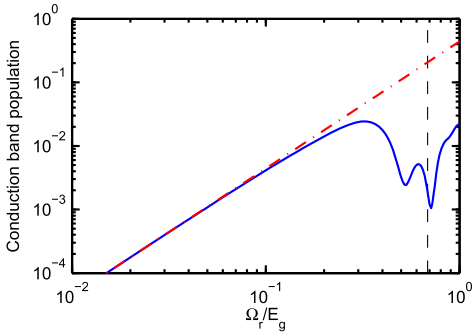

FIG. 3. Final dielectric conduction band population for the short pulse versus Ω_r/E_g, with $\beta = 6.3$ for the 2B (solid) and FVB solution (dash dot); for all other parameters, see Fig. 1(e); Ω_r is changed by varying the dipole moment d. The dashed line indicates Ω_r/E_g used in Fig. 1(e).

The resulting increase in the number of resonant photon channels yields smaller ranges of field strengths over which complete channel closing can occur [24]. This will render channel closing less important. As a result, in the mid-IR and longer wavelength regimes, optical field ionization in dielectrics is expected to resemble that of semiconductors; in our model, optical field ionization remains suppressed due to the dynamic Stark shift, which is independent of wavelength. In a more complete model, laser heating and impact ionization will become more important; electron energy and ionization through inelastic collisions increase as the quiver velocity grows, with F_0/ω_0. Particularly in long pulses, damage might occur before the dynamic Stark shift becomes relevant.

Finally, in a more complete description, many-body effects will need to be investigated. For example, electron-hole interaction modifies band gap and Rabi frequency [21], thus potentially influencing ionization.

*cmcdo059@uottawa.ca

[1] L. Keldysh, Ionization in the field of a strong electromagnetic wave, Sov. Phys. JETP **20**, 1307 (1965).

[2] M. Schultze *et al.*, Attosecond band gap dynamics in silicon, Science **346**, 1348 (2014).

[3] M. Schultze *et al.*, Controlling dielectrics with the electric field of light, Nature (London) **493**, 75 (2013).

[4] A. Schiffrin *et al.*, Optical-field-induced current in dielectrics, Nature (London) **493**, 70 (2013).

[5] F. Krausz and M. I. Stockman, Attosecond metrology: from electron capture to future signal processing, Nat. Photonics **8**, 205 (2014).

[6] T. T. Luu, M. Garg, S. Yu. Kruchinin, A. Moulet, M. Th. Hassan, and E. Goulielmakis, Extreme ultraviolet high-harmonic spectroscopy of solids, Nature (London) **521**, 498 (2015).

[7] V. E. Gruzdev, Photo-ionization rate in wide band gap crystals, Phys. Rev. B **75**, 205106 (2007).

[8] P. A. Zhokhov and A. M. Zheltikov, Field-Cycle Resolved Photoionization in Solids, Phys. Rev. Lett. **113**, 133903 (2014).

[9] P. G. Hawkins and M. Yu. Ivanov, Role of subcycle transition dynamics in high-order-harmonic generation in periodic structures, Phys. Rev. A **87**, 063842 (2013).

[10] R. R. Gattass and E. Mazur, Femtosecond laser micromachining in transparent materials, Nat. Photonics **2**, 219 (2008).

[11] M. F. Yanik, H. Cinar, H. N. Cinar, A. D. Chisholm, Y. Jin, and A. Ben-Yakar, Neurosurgery: Functional regeneration after laser axotomy, Nature (London) **432**, 822 (2004).

[12] M. Farsaril and B. N. Chichkov, Materials processing: Two-photon fabrication, Nat. Photonics **3**, 450 (2009).

[13] T. D. Gerke and R. Piestun, Aperiodic volume optics, Nat. Photonics **4**, 188 (2010).

[14] K. A. Pronin, A. D. Bandrauk, and A. A. Ovchinnikov, Harmonic generation by a one-dimensional conductor: Exact results, Phys. Rev. B **50**, 3473(R) (1994).

[15] S. Ghimire, A. D. DiChiara, E. Sistrunk, P. Agostini, L. F. DiMauro, and D. A. Reis, Observation of high-order harmonic generation in a bulk crystal, Nat. Phys. **7**, 138 (2011).

[16] M. Krüger, M. Schenk, and P. Hommelhoff, Attosecond control of electrons emitted from a nanoscale metal tip, Nature (London) **475**, 78 (2011).

[17] B. Zaks, R. B. Liu, and M. S. Sherwin, Experimental observation of electronhole recollisions, Nature (London) **483**, 580 (2012).

[18] M. Hohenleutner, F. Langer, O. Schubert, M. Knorr, U. Huttner, S. W. Koch, M. Kira, and R. Huber, Real time observation of interfering crystal electrons in high-harmonic generation, Nature (London) **523**, 572 (2015).

[19] G. Vampa, T. J. Hammond, N. Thiré, B. E. Schmidt, F. Légaré, C. R. McDonald, T. Brabec, and P. B. Corkum Linking high harmonic generation from gases and solids, Nature (London) **522**, 462 (2015).

[20] G. Vampa, T. J. Hammond, N. Thire, B. E. Schmidt, F. Legare, C. R. McDonald, T. Brabec, D. D. Klug, and P. B. Corkum, All-Optical Reconstruction of Crystal Band Structure, Phys. Rev. Lett. **115**, 193603 (2015).

[21] H. Haug and S. Koch, *Quantum Theory of Optical and Electronic Properties of Semiconductors*, 4th ed. (World Scientific Publishing, Singapore, 2004).

[22] C. R. McDonald, G. Vampa, P. B. Corkum, and T. Brabec, Interband Bloch oscillation mechanism for high harmonic generation in semiconductor crystals, Phys. Rev. A **92**, 033845 (2015).

[23] G. Vampa, C. R. McDonald, G. Orlando, D. D. Klug, P. B. Corkum, and T. Brabec, Theoretical Analysis of High Harmonic Generation in Solids, Phys. Rev. Lett. **113**, 073901 (2014).

[24] See Supplemental Material at http://link.aps.org/supplemental/10.1103/PhysRevLett.118.173601 for a derivation of the GK model and for a list of the parameters.

[25] M. Lewenstein, P. Balcou, M. Y. Ivanov, A. L'Huillier, and P. B. Corkum, Theory of high harmonic generation by low-frequency laser fields, Phys. Rev. A **49**, 2117 (1994).

[26] Note that the ionization from closing channels decays exponentially and with $\propto \mathrm{Im}[K_n]$. This can be neglected in most cases, except when all channels are closed and a channel comes close to, but misses, a reopening.

[27] R. W. Boyd, *Nonlinear Optics* (Academic Press, San Diego, 2003).